Exploiting the ANN Potential in Estimating Snow Depth and Snow Water Equivalent From the Airborne SnowSAR Data at X- and Ku-Bands

Exploiting the ANN potential in estimating Snow Depth and Snow Water Equivalent from the airborne SnowSAR data at X and Ku bands

E. Santi, Member, IEEE, M. Brogioni, Member, IEEE, M. Leduc-Leballeur, G. Macelloni, Member, IEEE, F. Montomoli, Member, IEEE, P. Pampaloni, Life fellow IEEE, J. Lemmetyinen, J. Cohen, H. Rott, Fellow, IEEE, T. Nagler, Member, IEEE, C. Derksen, J. King, N. Rutter, R. Essery, C. Menard, M. Sandells and M. Kern.

***Abstract*— Within the framework of European Space Agency (ESA) activities, several campaigns were carried out in the last decade with the purpose of exploiting the capabilities of multi-frequency Synthetic Aperture Radar (SAR) data to retrieve snow information. This paper presents the results obtained from the ESA SnowSAR airborne campaigns, carried out between 2011 and 2013 on boreal forest, tundra and alpine environments, selected as representative of different snow regimes. The aim of this study was to assess the capability of X and Ku band SAR in retrieving the snow parameters, namely Snow Depth (SD) and Snow Water Equivalent (SWE). The retrieval was based on Machine Learning (ML) techniques and, in particular, of Artificial Neural Networks (ANN). ANN have been selected among other ML approaches since they are capable to offer a good compromise between retrieval accuracy and computational cost. Two approaches were evaluated, the first based on the experimental data (data driven) and the second based on data simulated by the Dense Medium Radiative Transfer (DMRT). The data driven algorithm was trained on half of the SnowSAR dataset and validated on the remaining half. The validation resulted in a correlation coefficient $R \simeq 0.77$ between estimated and target SD, a root-mean-square error (RMSE) $\simeq$ 13 cm, and bias = 0.03 cm. ANN algorithms specific for each test site were also implemented, obtaining more accurate results, and the robustness of the data driven approach was evaluated over time and space.**

The algorithm trained with DMRT simulations and tested on the experimental dataset was able to estimate the target parameter (SWE in this case) with R=0.74, RMSE =34.8 mm and bias=1.8 mm. The model driven approach had the twofold advantage of reducing the amount of in-situ data required for training the algorithm and of extending the algorithm exportability to other test sites.

Index Terms — SnowSAR, Snow Depth, Snow Water Equivalent, SAR, Artificial Neural Networks, DMRT-QMS model.

I. INTRODUCTION

DESPITE the urgent need of an accurate characterization of snow cover for climate, hydrological and meteorological reasons, the existing observation systems are unable to provide detailed information of snow at the spatial and temporal resolution and accuracy required by stakeholders and users.

In-situ systems are unable to provide spatially distributed and frequent measurements for wide regions of the globe [1] and the possibility of monitoring snow from space is still limited by the absence of sensors able to measure key snow parameters at the required temporal and spatial resolution. Indeed, while the snow cover extent is routinely observed by multispectral sensors (e.g. [2]), the microwave satellite radiometers are the only instruments currently operating at the appropriate frequencies for retrieving information on snow mass at global scale (e.g. [3-6]). These sensors, although characterized by good coverage and temporal revisiting, are hampered by the spatial resolution which is in the order of tens of kilometres. Conversely, the Synthetic Aperture Radar (SAR), which could be suitable for snow mass monitoring at high spatial resolution, are in fact limited by the poor revisiting. Most important, the frequency bands on board of the current satellites, namely L, C and X bands, are not the optimal, and SAR sensors at higher frequencies would be better suited for this scope.

Nevertheless, some examples of Snow Depth (SD) and Snow Water Equivalent (SWE) retrieval using SAR can be found in literature. Among the others, Gunerussen et al. [7] attempted the retrieval by using a delta-K technique on interferometric synthetic aperture radar (InSAR) by utilizing the presence of scatterers in two images with and without snow cover. Pettinato et al. [8] exploited the Artificial Neural Networks to estimate SWE from Cosmo Sky-MED X band SAR. Finally, Leinss et al. [9, 10] applied differential interferometry to polarimetric

E. Santi, M. Brogioni, M. Leduc-Leballeur, G. Macelloni, F. Montomoli and P. Pampaloni are with the Institute of Applied Physics - National Research Council (IFAC – CNR), Italy. Email e.santi@ifac.cnr.it.

J. Lemmetyinen and J. Cohen are with the Finnish Meteorological Institute (FMI), Finland.

H. Rott and T. Nagler are with ENVEO Environmental Earth Observation Information Technology GmbH, Austria

C. Derksen and J. King are with Environment and Climate Change Canada (ECCC), Canada

N. Rutter is with Northumbria University (NU), United Kingdom.

R. Essery and C. Menard are with the University of Edinburgh (UE), United Kingdom

M. Sandells is with CORES Science and Engineering Limited (CORES), United Kingdom

M. Kern is with the European Space Research and Technology Centre (ESA/ESTEC), The Netherlands

This study was carried out under the European Space Agency Contract "SnowSAR Campaign Data Analysis Study", C4000118400/16/NL/FF/gp. This support is gratefully acknowledged.

SAR data at X band from TerraSAR-X. Although the most part of the scientific community agrees in considering the C-band SAR not suitable for SD/SWE monitoring, the mapping of SD in the Northern Hemisphere mountains by using Sentinel-1 has been recently proposed by Lievens et al. [11]. This study can be regarded as one of the first attempts to apply a retrieval methodology based on SAR data at global scale.

The CoReH2O (Cold Regions Hydrology High-resolution Observatory) satellite mission, candidate for the European Space Agency (ESA) 7th Earth Explorer [12] aimed to address these issues by providing timely information on SWE over land at a resolution of few hundred of meters. The sensor envisaged for CoReH2O was a dual polarization, dual frequency SAR at X (9.6GHz) and Ku (17.25GHz) bands. To demonstrate the CoReH2O retrieval concept, ESA developed the SnowSAR airborne SAR simulating the satellite sensor [13-14]. Between 2010 and 2013, experimental campaigns have been carried out in several sites in Northern Finland, Austrian Alps, and Northern Canada.

Although a comprehensive analysis of the entire dataset was not provided yet, SnowSAR data collected in specific test areas were already analysed in previous works [15-20, 23]. In [20], a retrieval approach based on a parametrized implementation of the BIContinuous Dense Media Radiative Transfer Model (Bic-DMRT) [21-22] was applied to SnowSAR data collected both in Finland and Canada. In [23], the SWE retrieval from SnowSAR data was attempted for Finland test area by minimizing the difference between simulated and measured backscatter, as a function of SWE and the effective snow grain size (RE). The backscattering was simulated by a semi-empirical radiative transfer (RT) model.

In this study, SnowSAR acquisitions from all test sites have been compared with in situ measurements of snow parameters, with the aim of exploiting the capability of these frequencies in estimating SD and SWE. Based on the results of the sensitivity analysis, the retrieval of both SD and SWE has been then attempted with an algorithm based on the Artificial Neural Networks (ANN). With the increasing computational power of recent computers, Machine Learning (ML) in general, and ANN in particular, gained an exponentially increased consideration for solving a wide range of problems [24]. Since the late 80's, the ANN capabilities of approximating nonlinear relationships and solving a variety of mathematical problems were largely proven [25-26]. Several examples of ANN applications to remote sensing of hydrological parameters can be found in literature. In particular, ANN applications to SAR and microwave radiometers for the retrieval of surface parameters are shown in [27-32]. A few ANN applications for the retrieval of SWE from SAR data can be also found [8]. With respect to other Machine Learning (ML) techniques, the ANN have proven to be able to offer a good compromise between retrieval accuracy and computational cost [30]. This study pointed out the ANN capability of exploiting the synergy of frequencies and polarizations of SnowSAR acquisitions to improve the retrieval with respect to the algorithms based on single frequency and single polarization. The possibility of training the ANN with experimental data (experimental driven training) and with data simulated by an electromagnetic forward model (model driven training) have been both evaluated. To this scope, the model simulations have been based on the Dense Medium Radiative Transfer (DMRT) Theory with the Quasi Crystalline approximation of densely packed Sticky spheres (DMRT-QMS) [33-34].

The paper is structured as follows: a synthetic description of the experimental campaigns and datasets is provided in section II, and the sensitivity analysis of SnowSAR data to SD is presented in section III. Both the data driven and the model driven retrieval algorithms are described in Section IV and their results are presented in section V, where a retrieval based on single frequency is also shown. Finally, the obtained results are discussed in section VI, focusing on the effectiveness of the proposed approach.

II. SNOWSAR DATASET

SnowSAR is a side looking, dual polarized (VV/VH), SAR instrument designed to operate from small airplanes. In the framework of CoReH2O preparatory experiments, some flight campaigns have been carried out between 2010 and 2013 using SnowSAR in several sites in Northern Finland, Austrian Alps and Northern Canada. The main information about the SnowSAR campaigns is summarized in this section, for a complete description, see the detailed documentation of each campaign [15-16, 35-36].

The purpose of the SnowSAR campaigns was to gather information on the backscattering properties of snow-covered terrain and to demonstrate the CoReH2O retrieval concept. SnowSAR was flown in Sodankylä, Northern Finland for a single test flight in 2011 and a total of ten flights during the winter 2011-2012. The Sodankylä site represents a typical northern boreal forest environment, consisting of a mosaic of coniferous-dominated forests, wetlands and lakes [16]. Additional acquisitions considered in this study took place over a tundra site (Saariselka). Over the Austrian Alps, three flight campaigns were performed between November 2012 and February 2013 over three sites located in different elevation zones, namely Leutasch, representing an Alpine valley with cultivated meadows at 1100 m above sea level, Rotmoos, a narrow valley above the tree-line covered alpine grassland, bogs, debris and moraines at elevations between 2250 and 2400 m, and Mittelbergferner, a glacier extending from 2500 m to 3550 m in elevation. In Canada a total of two missions were flown in March and April 2013, over a site in Trail Valley Creek, near Inuvik, Northwest Territories, Canada. Trail Valley Creek, located at the Northern edge of the Boreal forest, is representative of the tundra environment and snow regime.

The SD measured during the experiments ranged between 0 and <150 cm for both Finland and Canada and from 0 to 280 cm for Alps. Fig. 1 shows the SD distribution for each test area.

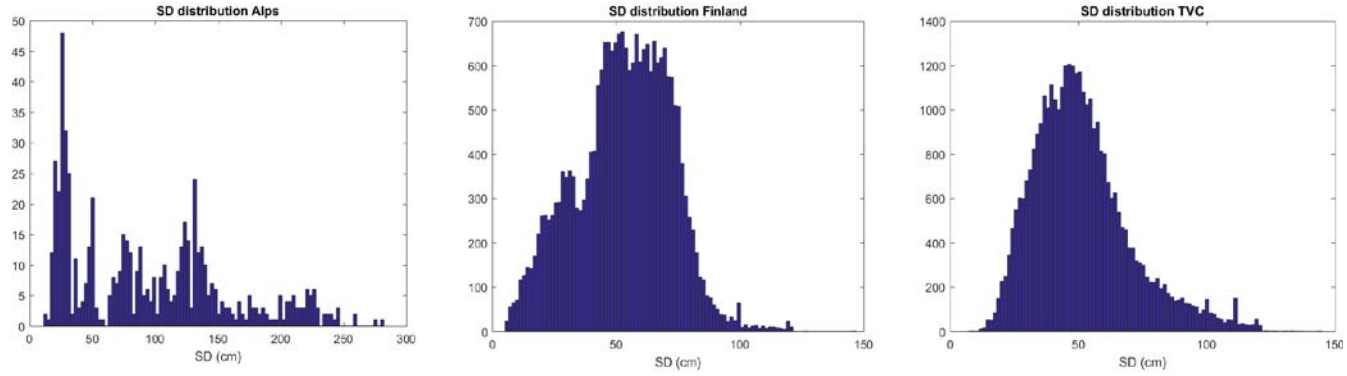

a) b) c)

Fig. 1. Distribution of the in-situ SD measurements collected during the experiments in a) Alps, b) Finland, c) Canada.

At a flight altitude of 1200 meters, the SnowSAR swaths span approximately 400 meters in range and up to several kilometers in the flight direction, while the calibrated and geocoded backscattering coefficient (σ^0) are provided at a spatial resolution of 2 and 10 meters. The instrument calibration was performed by a combination of internal calibration, corner reflector targets installed along flight paths, and cross-calibration with space-borne instruments [14].

The SnowSAR dataset is publicly available: the calibrated and geocoded σ^0 it can be requested through the ESA data portal (https://earth.esa.int/web/guest/campaigns).

Simultaneously with flights, in-situ snow measurements were performed in each test site: The majority of data consisted of snow depth (SD) punctual measurements sampled along transects at a minimum interval of 100 m. Measurements of snow profile were also carried out, including vertical profiles of snow density, temperature, hardness, wetness, grain size and shape. SWE measurements were available for a subset of points in Finland and Canada areas [15, 16] and from the snow pit measurements of the Alpine test sites [17]: the snow density derived from the ratio SWE/SD was in the range 100 – 450 Kg/m^3.

TABLE I. COMPOSITION OF THE DATABASE: N. OF POINTS PER TEST SITE IN EACH TEST AREA

Test area	SD range (cm)	Test site	n. of data (4 σ^0 +SD)	n. of data (4 σ^0 +SWE)
Alps	0 - 280	Leutasch	87	-
		Mittelbergferner	105	-
		Rotmoos	419	-
Finland	0 - <150	Sodankylä	12400	390
		Saariselka	3585	50
Canada	0 - <150	TVC	24081	405
		Total	40677	845

For the scopes of this study, the SnowSAR acquisitions have been co-located with in-situ data by relating each measurement to the 3x3 average of SnowSAR acquisitions centered in the measurement point. The resulting dataset was composed of ≃40,000 sets of 4 σ^0 values (X and Ku bands, VV and VH pol.) and corresponding SD in situ. The total amount of data for each test site is summarized in Table I: most of the data were collected in Canada and Finland where SD did not exceed 150 cm, while SD values up to 280 cm were recorded in the alpine dataset, which represents the 1.5% of the entire dataset.

III. DATA ANALYSIS

A. *Backscattering vs. incidence angle*

The σ^0 signature depends on the wide range of local incidence angles on which SAR data have been acquired (between 25° and 65°). The angular dependence was found to be particularly important for the Alpine test area, in which the Local Incidence Angle (LIA) differ significantly from the nominal angle because of the complex topography. In this area, the backscatter exhibited a decreasing trend when LIA increases, with a correlation coefficient R up to -0.59 for X data in VV polarization. The expected decrease of σ° for increasing LIA was confirmed in the Finnish test sites, characterized by almost flat topography, with R ≃ -0.33.

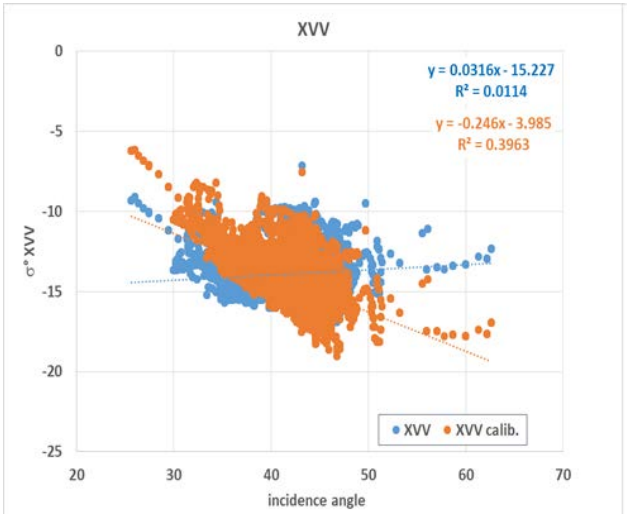

Fig. 2: The behavior of the SnowSAR backscattering vs. LIA before and after normalization for Canada test site.

The Canada dataset exhibited an unexpected increasing trend of σ° with increasing LIA. Such increase depended on the use of the nominal incidence angle instead of LIA for computing σ^0. The backscattering computation was therefore revised to include a correction factor expressed as $\frac{\sin(\vartheta_{local})}{\sin(\vartheta_{nominal})}$.

The trends of σ^0 as a function of LIA before and after applying the correction are displayed in Fig. 2: for simplicity, figure refers to X band in VV polarization, but analogous results have been obtained for both frequencies and polarizations.

The correlation coefficients between σ° and LIA are summarized in Table II, the R values listed for Canada refer to the LIA-corrected σ^0.

TABLE II. R VALUES OF THE CORRELATION BETWEEN SNOWSAR DATA AND LOCAL INCIDENCE ANGLE (LIA)

	R			
	X VV	X VH	Ku VV	Ku VH
Alps	-0.59	-0.3	-0.44	-0.22
Finland	-0.24	-0.1	-0.33	-0.02
Canada	-0.62	-0.54	-0.33	-0.59

B. Backscattering vs. SD

Considering the entire SnowSAR dataset, the σ^0 values at single frequency and polarization were found poorly correlated to the in-situ SD and SWE. This result agrees with previous studies [23] and it depends on the temporal and spatial variability of other snow parameters that affect the relationship σ° - SD, i.e.: snow density, grain radius and stratigraphy, as well as on the medium (soil, vegetation, debris, glacier ice) underlying snow.

The σ° sensitivity to SD was evaluated for each test area, revealing site-dependent relations: for example, at the Mittelbergferner glacier, σ° at both frequencies and polarizations is negatively correlated to SD between Mission 1 (M1, 21 Nov. 2012) and Mission 3 (M3, 21 Feb. 2013), because, between the two dates, the strong signal from the coarse-grained frozen firn and glacier ice is attenuated by the increase of seasonal snow [36]. At Leutasch instead, the relation between σ° and SD is positive due to the strong backscattering signal of coarse-grained snow caused by melt-freeze metamorphosis of snow over the smooth ground [36].

Some increase of backscattering with SD was found for Finland and Canada test sites: slightly higher correlation was found at X band for the deeper SD in Finland and at Ku band for the shallower SD in Canada, respectively. However, the R values are too low for drawing any conclusion about.

TABLE III. CORRELATION BETWEEN SNOWSAR σ° AND SD: R VALUES FOR EACH AREA AT EACH FREQUENCY AND POLARIZATION.

	R			
	X VV	X VH	Ku VV	Ku VH
Leutasch	0.81	0.73	0.65	0.73
Mittelbergferner	-0.6	-0.02	-0.6	-0.39
Rotmoos	-0.05	0.05	-0.43	-0.36
Finland	0.22	0.34	0.07	0.12
Canada	≃ 0	0.12	0.19	0.27
All	0.15	0.26	0.1	0.26

The R values obtained at each frequency and polarization for each test site are listed in Table III. The sensitivity analysis was repeated for the data collected in the central incidence angles (35° to 45°), in order to reduce the effect of LIA on the σ^0 sensitivity to SD. However, the results did not point out any significant increase of correlation.

IV. ANN RETRIEVAL ALGORITHMS

The sensitivity analysis clearly confirmed that a general relationship between σ° at single frequency and polarization and SD cannot be established on the entire dataset, since many other factors concur to the total signal measured by SnowSAR. The spatial and temporal variations of soil background and of the other snow parameters, have indeed a dominant effect, which was capable of masking the σ° sensitivity to the target parameter. However, the effect of each soil and snow parameter on the measured σ° depended on frequency and polarization. Therefore, the synergy of available polarizations and frequencies was exploited in this study, with the aim of improving the retrievals.

For this scope, the SD/SWE retrievals were based on Feed-Forward Multi-Layer Perceptron ANN (FF-MLP), because of their intrinsic capability of make synergic use of multiple inputs.

FF-MLP are composed of one or more hidden layers with a certain number of neurons (also called perceptrons), that are fully interconnected. The inputs are transferred from a layer to another by the transfer function: linear, hyperbolic tangent sigmoid (tansig), and logistic sigmoid (logsig) are the most popular transfer functions. The ANN training is based on the so-called Back Propagation learning rule (BP), which attempts to minimize the mean square error (MSE) between the target value and the training output. Such minimization is obtained by adjusting the weights and offsets to inhibit or excite the connections: this is achieved iteratively during the training. The ANN implementation proposed in this study was based on the Matlab® Neural Networks toolbox.

A SD retrieval algorithm based on ANN has been therefore implemented and validated using the available dataset. The main constraint for obtaining good accuracies with ANN algorithms, is represented by the statistical significance of the training set, which shall be representative of all the surface conditions that can be encountered in the operational use of the algorithm [37]. ANNs are prone to outliers: it means that the predicted output can be affected by large errors if the input data are outside the range of values that ANN learned to manage during the training. This ANN characteristic could some limitations to the algorithm exportability, in this case to the possibility to use the already trained ANN for predicting SD in other test areas.

Two different strategies have been evaluated, training the algorithm with a subset of the experimental data available (experimental driven approach), and with data simulated by electromagnetic models (model driven approach), the latter aimed at overcoming any possible limitation to the algorithm exportability. Indeed, by employing simulated data in the

training, the ANN acts for retrieving the target parameter by inverting the electromagnetic model, similarly to other physically based algorithms, but with less constraints due to the approximations needed for an analytical inversion [38].

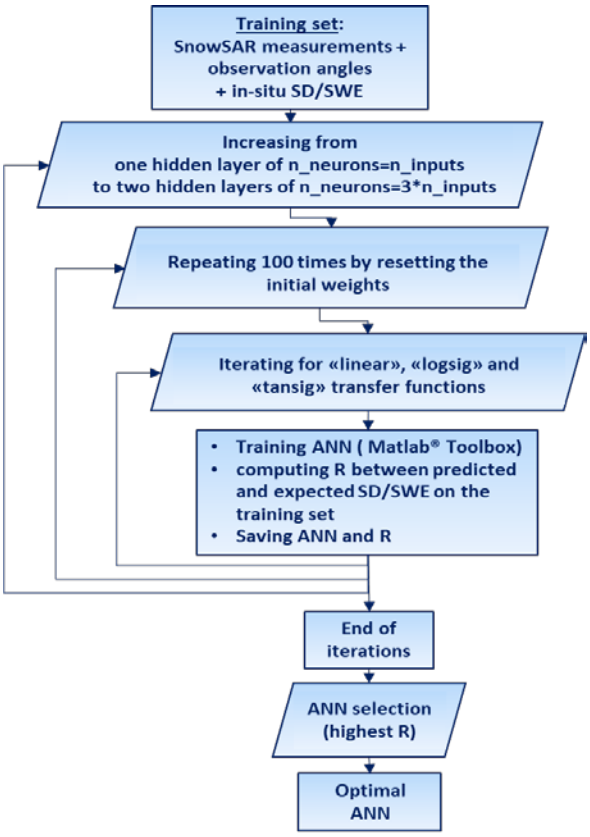

Fig. 3. Iterative process for defining the "optimal" ANN

Algorithm inputs were the SnowSAR acquisitions at both frequencies and polarizations and the corresponding LIA, in order to account for the backscattering dependence on the local topography. Considering that the number of SWE measurements was not sufficient for implementing the data driven approach, the algorithm outputs was SD in the case of data driven approach and SWE in the case of model driven approach. In both experimental and model driven approaches, the optimal ANN for the given problem was defined by applying the systematic search described in [39]. The process increased iteratively the number of neurons and hidden layers and tests the three transfer functions available with the scope of preventing the overfitting and the underfitting. The flowchart of Fig. 3 shows how the systematic process has been adapted to this study. The optimal ANN resulting from the iterative process was composed by two hidden layers of 14 neurons each, the transfer function was tansig.

A. Experimental driven approach

The three SnowSAR datasets summarized in Table I were divided in two equal parts: the first part was used for training the algorithm and the other part for validating the results, by predicting SD from the SnowSAR data not considered for the training. Both interleaved and random samplings have been considered for dividing the data in training and validation subsets: a negligible difference in the obtained results was found if using one or another sampling. In order to verify the statistical independence between training and validation, the correlation of σ° values from the two datasets corresponding to the same (or closest) SD vas evaluated. The obtained $R < 0.3$ at both frequencies and both polarizations confirmed the scarce correlation between training and validation datasets.

The training set was further divided in three parts, the first one served to iteratively define the weights and biases by applying the BP rule and the other two for having independent tests at each training iteration. In this study the percentages of data in the three subsets were 60%, 20% and 20% respectively.

B. Dedicated algorithms

The site dependent sensitivity of σ° to SD suggested that dedicated algorithms for Alps, Finland and Canada could improve the retrieval. Therefore, three ANN – one for each area – have been implemented and trained according to the processing described in the previous section, but considering only data from each test site. The optimal ANN for the Finland and Canada datasets was composed by two hidden layers of 10 to 12 neurons, respectively. Almost equivalent results were obtained by using logsig or tansig transfer functions. Depending on the small amount of data for the alpine dataset (611 data samples), the ANN for SnowSAR data on Alps was limited to one hidden layer of 7 neurons, in order to have a numbers of ANN parameters to be defined lower than the dimension of the training set (50% of the data available), thus preventing the problem to be indeterminated. In this way, it was possible to keep a subset of $\simeq$ 300 points not involved in the training for validating the results.

C. Model driven approach.

An implementation of the Dense Media Radiative Transfer (DMRT) theory, based on the Quasi-Crystalline Approximation (QCA) of Mie scattering of densely packed Sticky spheres [33, 34] was considered for implementing the model driven approach. The model, called DMRT-QMS, was developed by a team of the University of Washington (UW), United States and it is available online [40].

The input parameters required by DMRT-QMS are frequency, incidence angle, snow parameters, namely thickness, grain diameter, snow density, and stickiness. The latter parameter accounts for the backscatter properties of natural snow packs, referring to distinct differences in sintering and clustering associated with different grain types and metamorphic states [41]. The contribution of soil under snow to the total backscattering was simulated by the Oh model [42].

Besides the observation angle, the model requires as inputs the soil permittivity and the surface roughness: the latter is expressed with a simplified parametrization based on Root Mean Square of the heights (rms). DMRT-QMS was run by considering an equivalent "single layer" snowpack, with average values of the input density and equivalent grain diameter, since detailed information on snow stratigraphy was

not available for the most part of dataset.

The DMRT-QMS was first calibrated on the experimental dataset: for this scope, the subset of 845 data, derived from the Finnish and Canadian in-situ measurements carried out during the experimental campaigns, was considered: this subset includes also the snow density information, which is a mandatory input for DMRT-QMS. The dataset was divided in two parts by random sampling: the first part served to adjust the model parameters and the second to validate the results. The model parameters were calibrated via RMSE minimization between simulated and measured backscattering, as a function of equivalent grain diameter, stickiness and soil surface roughness. For the minimization, the two snow parameters were kept free in the range 0.1 - 2.6 mm and 0.1 – 0.4, respectively, while the roughness parameter was kept free in the range 0.1 ÷2 cm. The range defined for grain size included the typical variability of snow grain dimensions [43, 44], while the one for stickiness was set according to the DMRT-QMS theory and previous studies [41, 45]. The other DMRT-QMS inputs were derived from the experimental dataset: in particular, SD ranged between 5 and 150 cm, and snow density ranged between 100 and 450 450 Kg/m^3. Finally, the soil under snow was assumed frozen, with permittivity $\varepsilon =$ 5.13+0.45i at X band and $\varepsilon =$4.91+0.49i at Ku band, according to the Mironov model [46]. The DMRT-QMS inputs for this minimization are summarized in Table IV.

TABLE IV. LIST OF THE DMRT-QMS MODEL INPUTS

bands	X and Ku (SnowSAR)
Incidence angle	Between 25° and 55°, from dataset
n. of snow layers	One “single layer” equivalent
Snow density	100 ÷450 kg/m^3, from in-situ measures
Equivalent grain diameter	0.3 ÷ 2.6 mm, from RMSE minimization.
Stickiness	0.1 ÷ 0.4, from RMSE minimization.
Snow temperature	Fixed = -10°C (small effect on simulations)
Snow depth	5 ÷ 150 cm, from in-situ measurements
Soil roughness (rms)	0.1 ÷2 cm from RMSE minimization
Soil dielectric constant	ε= 5.13+0.45i at X band and ε =4.91+0.49i at Ku band, according to Mironov model

The consistency between model simulations and experimental data has been verified by direct comparison: Fig. 4 shows the simulated backscattering as a function of SnowSAR measurements at both frequencies and polarizations, while the main statistics of the comparison between model simulations and SnowSAR data are summarized in Table V.

TABLE V. R, RMSE AND BIAS OF THE COMPARISON BETWEEN DMRT SIMULATIONS AND SNOWSAR ACQUISITIONS.

	R	RMSE (dB)	Bias (dB)
X VV	0.99	0.2	≃ 0
X VH	0.99	0.4	-0.02
Ku VV	0.91	0.7	-0.01
Ku VH	0.86	1.2	0.07

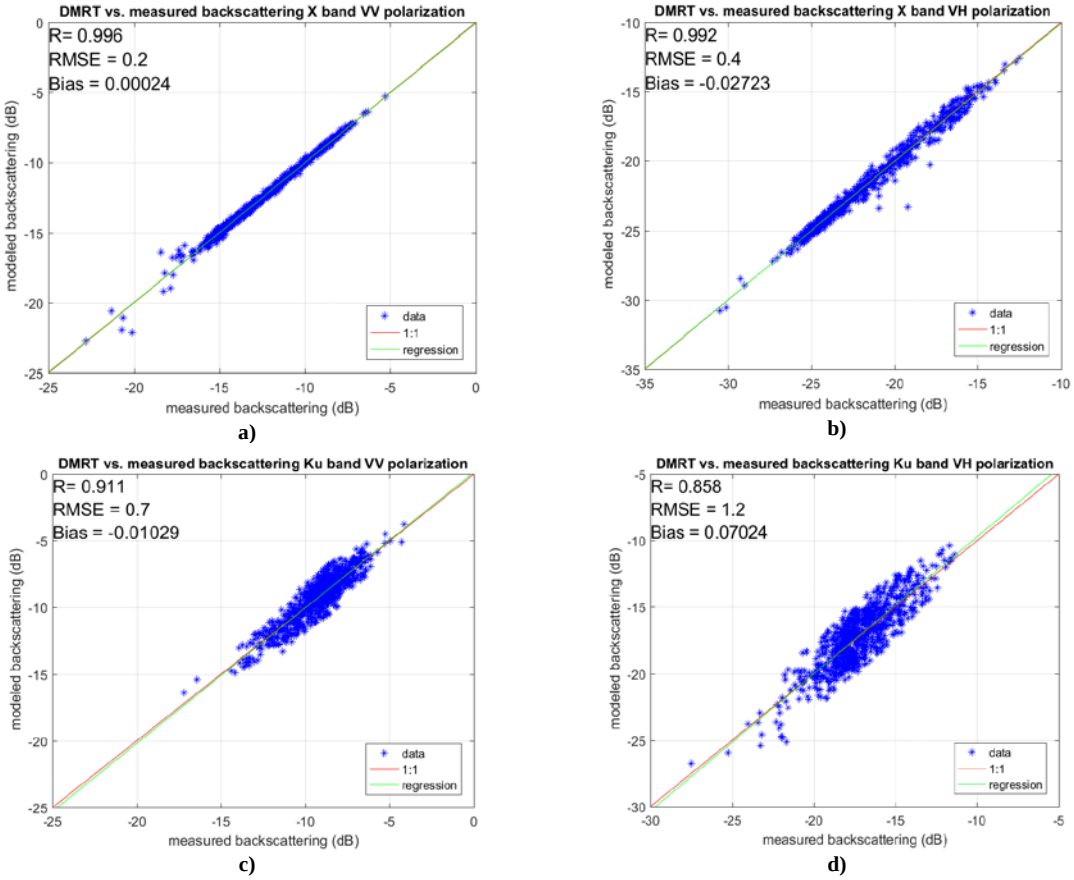

Fig. 4. DMRT-QMS simulations vs. SnowSAR measurements: a) XVV, b) XVH, c) KuVV and d) KuVH

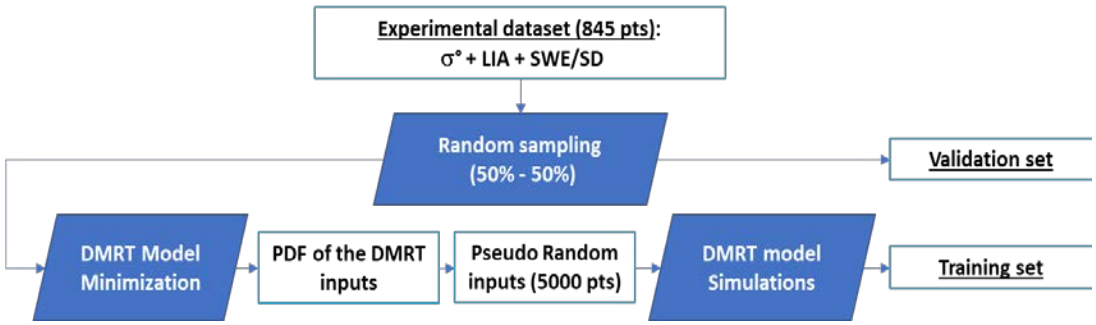

Fig. 5. Generation of the training and validation sets for the model driven approach.

The slightly worse result obtained at Ku band, can be attributed to the validity limits of the Oh model, which was used to simulate the soil background σ°. Indeed, the simplified parametrization for soil roughness works well for the lower microwave frequencies e.g. L- and C- bands; however, it is less accurate at higher frequencies and in particular at Ku-band [42]. At the latter frequency indeed, the modeled soil σ° shows an increase of several dB when the soil rms increases from 0 to 0.5 cm. Then σ° saturates almost completely, becoming insensitive to higher rms. This effect is only attenuated by the snow cover, but it is not cancelled. Therefore, in the range 0÷0.5 cm, small rms variations can lead to large variations of the modelled σ°. Conversely, in the range 0.5÷2 cm (or greater), the soil contribution at Ku band becomes insensitive to the surface roughness and it only depends on the observation angle. This odd sensitivity to the soil rms leads to some dispersion of simulated σ° values at Ku band, that affects the overall result.

After the minimization, the PDF distribution of all the inputs was computed and the pseudo random dataset was generated. Finally, the DMRT-QMS simulations were iterated using the pseudo random inputs to generate the training set. The process is summarized in the flowchart of Fig. 5.

The dataset obtained by iterating the model simulations was considered for training a new ANN, that was subsequently validated on the remaining 50% of the experimental dataset. The architecture definition followed the same iterative process of the experimental driven training, and the ANN inputs were the same; however, considering the availability of SWE data for this subset, the output parameter was SWE instead of SD.

V. Results

A. Experimental driven approach

The algorithm validation was obtained by applying the trained ANN to the validation set, composed of the 50% data not used in the training. Fig. 6 shows the SD estimated by the ANN algorithm as a function of the measured SD values in the validation dataset.

The corresponding statistics were: regression coefficient R ≃ 0.77, RMSE ≃ 13 cm, and a negligible bias. The clusters of data belonging to each dataset are evidenced by different colors. The result shown in Fig. 6 demonstrates that the algorithm, trained on ≃ 20.000 sets of backscattering vectors and corresponding SD, was able to estimate SD in the range 0-280 cm on the remaining ≃ 20.000 sets not involved in the training.

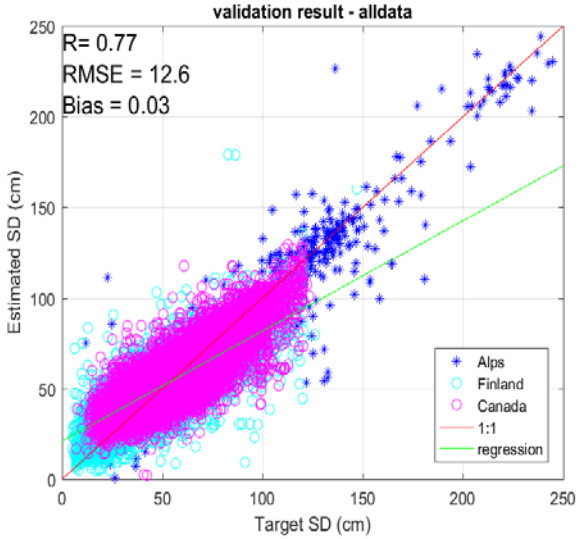

Fig. 6. ANN validation results as: a) scatterplot of the ANN estimated SD against target values.

1) Validation of the dedicated algorithms

The results obtained by the three dedicated algorithms are shown in Fig. 7 a) for Alps, b) for Finland and c) for Canada, respectively. In Fig. 7 b) and c) the results are represented as density plot, with color bar proportional to the occurrence of points. With respect to the results of the general ANN, the correlation increased for all the areas and RMSE decreased for Canada and Alps. The validation for Alps dataset was carried out on a small dataset (≃ 300 points), depending on the small amount of data available for the alpine dataset (611 data samples). The main results of the dedicated algorithms are summarized in Table VI.

Table VI. R, RMSE and Bias of the "dedicated" algorithms

	R	RMSE	Bias
Alps	0.9	25.6	3.4
Finland	0.86	10.1	0.03
Canada	0.7	10.5	0.03

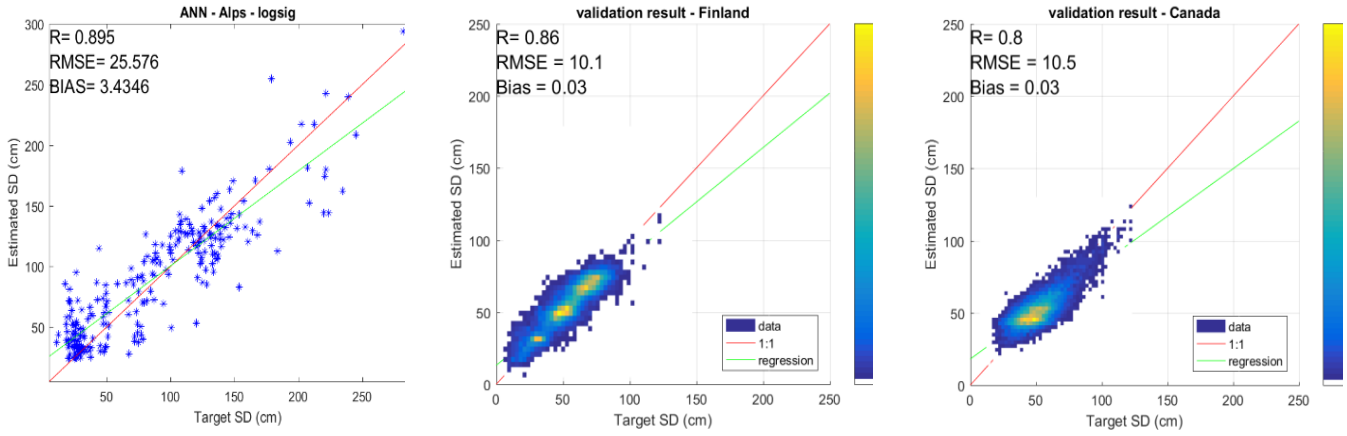

a) b) c)

Fig. 7. Validation of the "dedicated" ANNs: a) scatterplot estimated vs. target for the Alpine dataset, b) density plot estimated vs. target for the Finland dataset and c) density plot estimated vs. target for the Canada dataset. In b) an c) the colorbar is proportional to the occurrence of data.

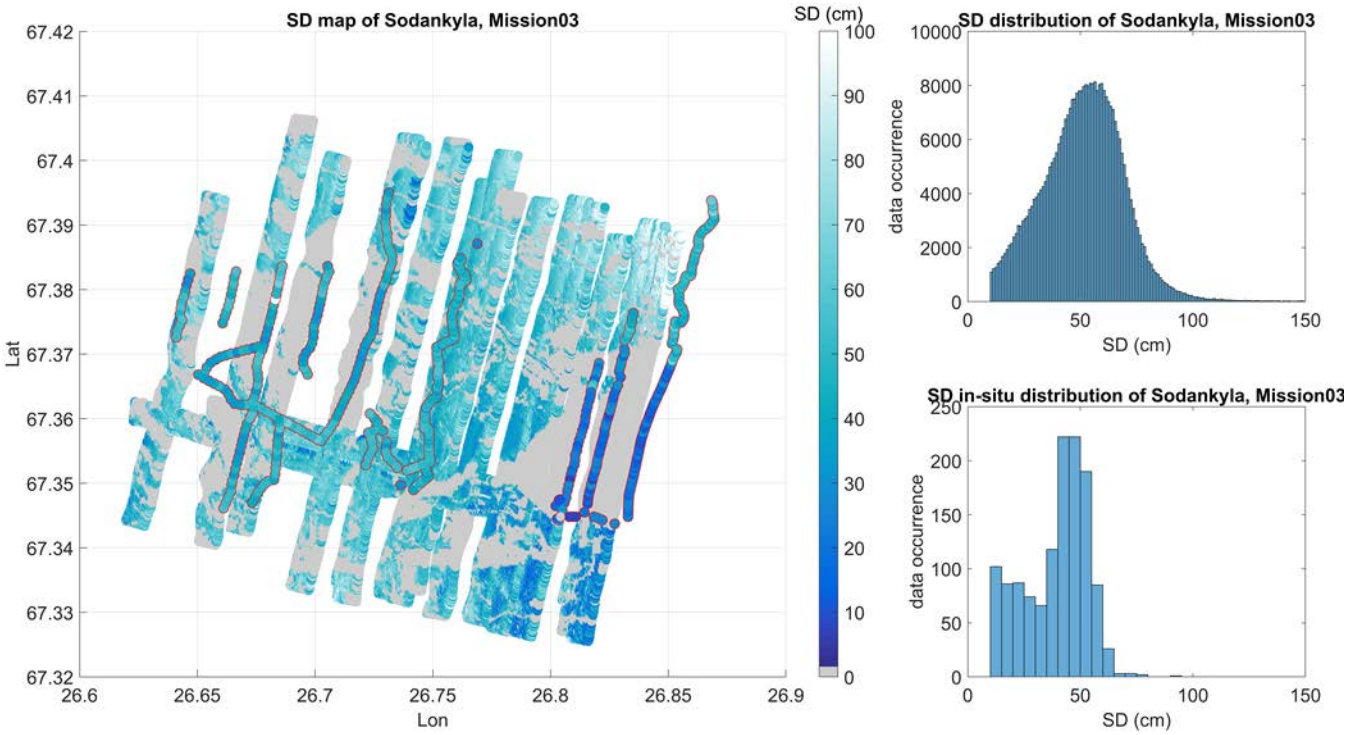

a)

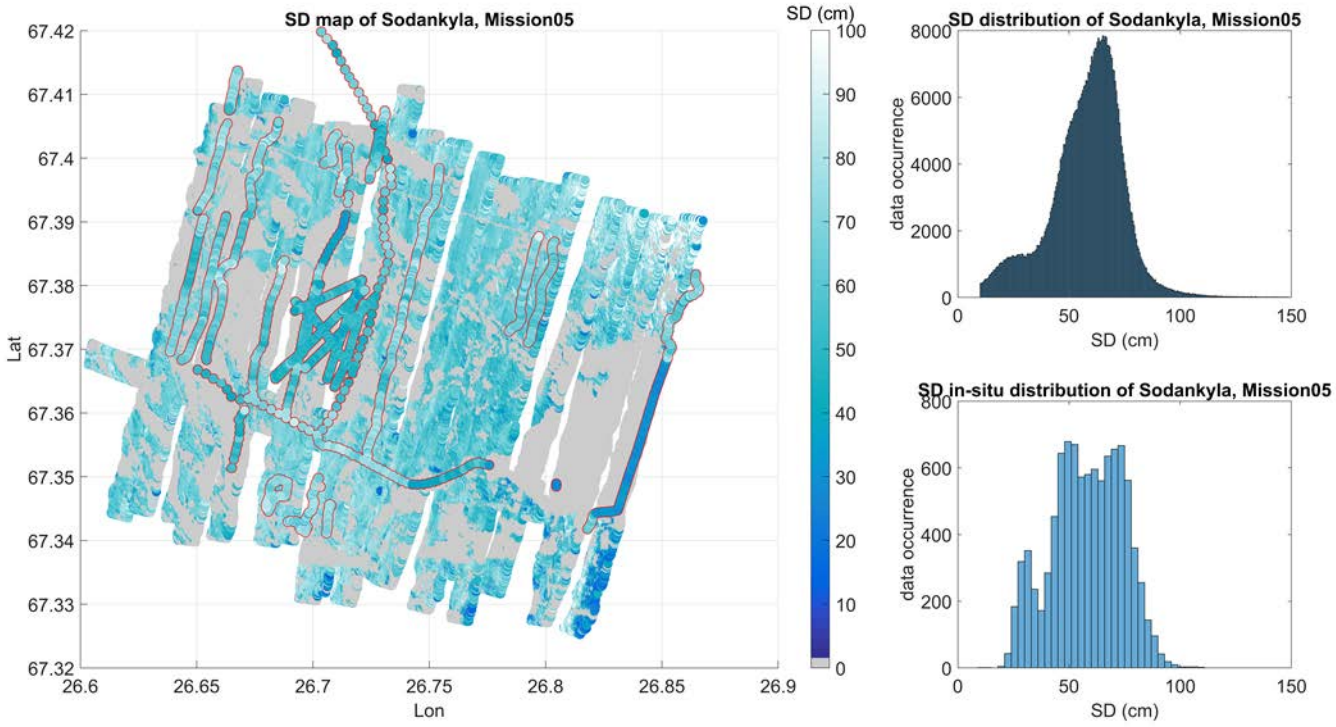
SD map of Sodankyla, Mission05
SD (cm)
Lat
Lon
SD distribution of Sodankyla, Mission05
data occurrence
SD (cm)
SD in-situ distribution of Sodankyla, Mission05
data occurrence
SD (cm)

b)

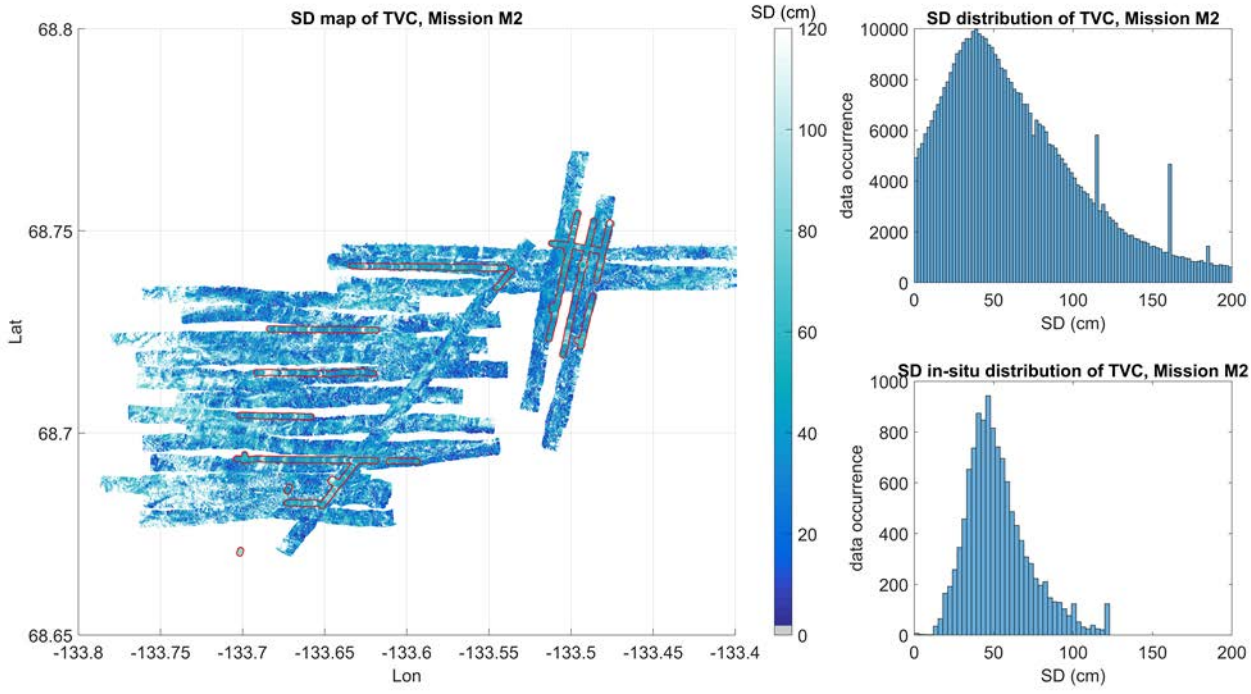
SD map of TVC, Mission M2
SD (cm)
Lat
Lon
SD distribution of TVC, Mission M2
data occurrence
SD (cm)
SD in-situ distribution of TVC, Mission M2
data occurrence
SD (cm)

c)

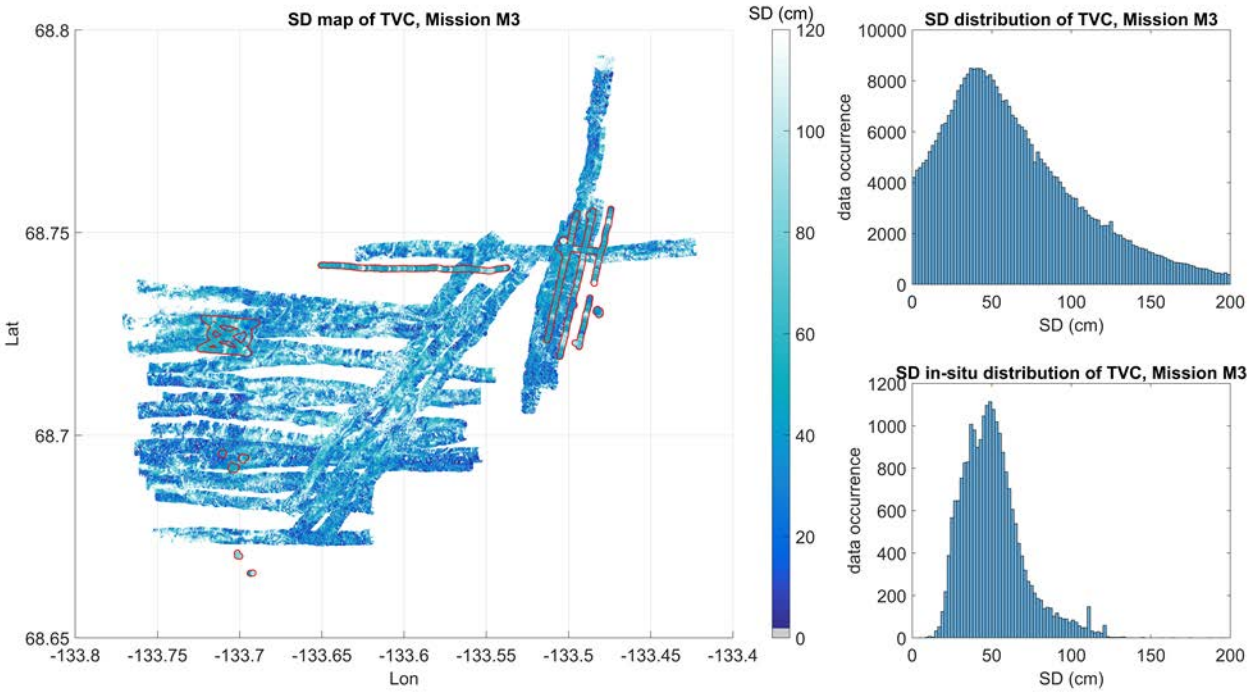
SD map of TVC, Mission M3
SD (cm)
Lat
Lon
SD distribution of TVC, Mission M3
data occurrence
SD (cm)
SD in-situ distribution of TVC, Mission M3
data occurrence
SD (cm)

d)

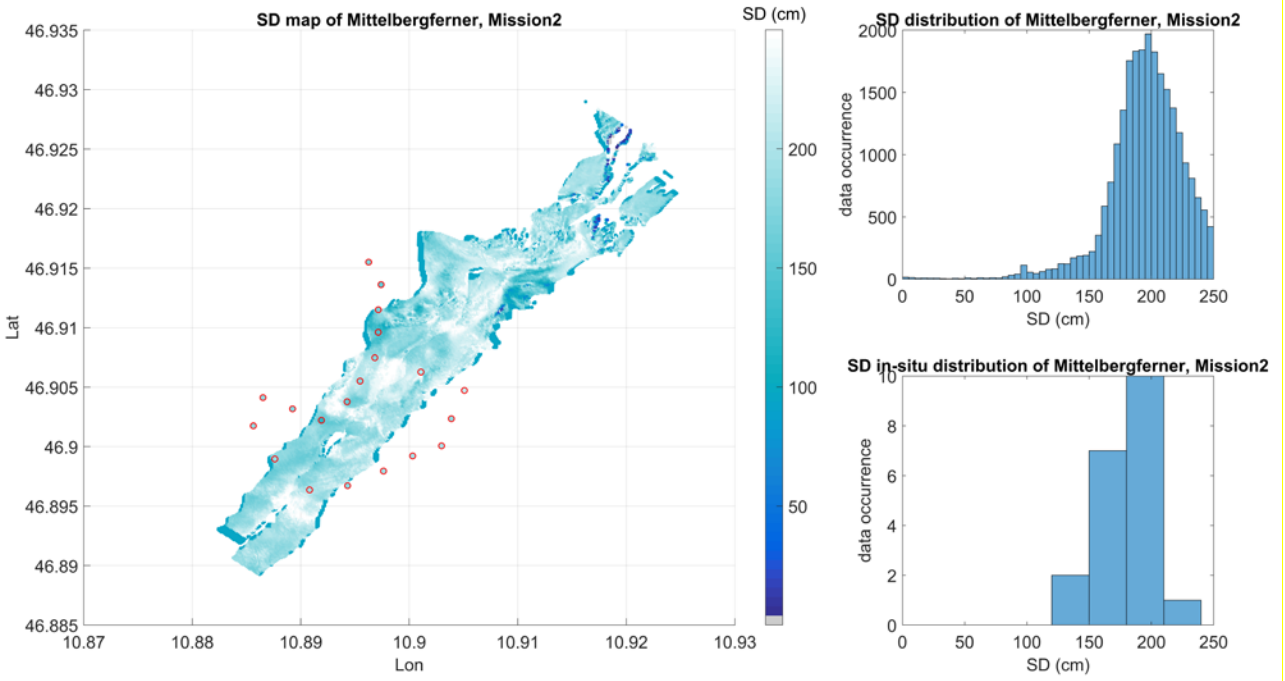
SD map of Mittelbergferner, Mission2
SD (cm)
Lat
Lon
SD distribution of Mittelbergferner, Mission2
data occurrence
SD (cm)
SD in-situ distribution of Mittelbergferner, Mission2
data occurrence
SD (cm)

e)

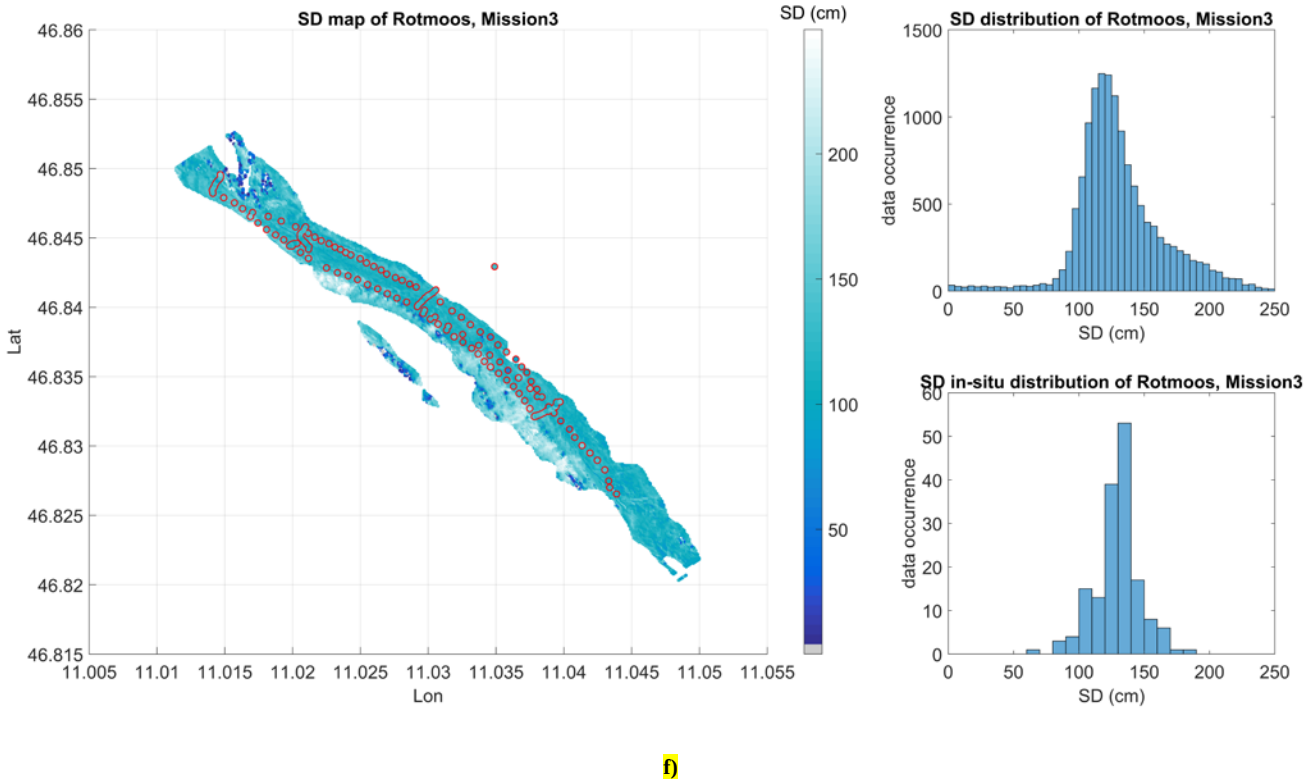

f)

Fig. 8. Snow depth maps: a) and b) Sodankylä test area, mission 3 and 5, c) and d) Canada test area, mission 2 and 3, e) Mittelbergferner mission 2 and f) Rotmoos mission 3. Areas with forest cover fraction > 25% for Sodankylä are masked in gray color. Each figure shows on the left the SD map generated by the ANN using SnowSAR data. Superimposed on the map are the SD values from the in-situ measurements, represented at circles with the same color scale of the map surrounded by a red line. The right top panel shows the distribution of SD values in the map and the right bottom panel shows the corresponding distribution of in-situ SD.

2) SD maps

To evaluate the generalization capabilities of the proposed method, the dedicated algorithms have been applied to the entire SnowSAR images, for generating output maps of SD at the same resolution of the input SnowSAR data.

Six examples of snow depth maps derived from SnowSAR flights on Sodankylä (Finland), Trail Valley Creek (Canada), Mittelbergfernel(Alps) and Rotmoos (Alps) are represented in Fig. 8. The color bar is proportional to SD, maps of Sodankylä were masked (gray color) for forests with cover fraction higher than 25%, according to [47].

Each figure shows on the left the SD map generated by the ANN using SnowSAR data. The distribution of SD values estimated by the ANN is represented in the right top panel and the right bottom panel shows the corresponding distribution of in-situ SD. Superimposed on the maps are the SD values from the in-situ measurements, represented with the same colour scale surrounded by a red line. The agreement between estimated and measured SD can be qualitatively deducted from the comparison of the SD values estimated by the ANN and the values measured along the transects, although in some cases the transects were not covered by the SnowSAR paths.

The maps were validated with the in-situ measurements available at each date, obtaining $0.76 \leq R \leq 0.8$ and 6 cm $\leq$ RMSE $\leq$ 10 cm, for the Canada and Finland test areas, $0.85 < R < 0.9$ and 0.2<RMSE <25 cm for the Alp test area. The SD distribution outside the validation points agreed with the qualitative reports from the experimental campaigns.

3) Algorithm robustness over time: Finland test case

In order to point out any site dependencies of the data driven approach, the algorithm exportability was evaluated over time by focusing on the Sodankylä test area (Finland). The available dataset was divided in two consecutive subsets: the first (SUB1) was composed of data from mission 1 to mission 5, corresponding to a significant evolution of the snow conditions, with an SD increase from 0 to 90 cm. The second subset (SUB2) was instead composed of data from mission 6 to mission 10, corresponding to relatively stable snow conditions until the beginning of snow melting.

The retrieval has been attempted by implementing two different ANNs: the first trained with the SUB1 dataset and tested on SUB2 and the second trained with SUB2 and tested on SUB2.

The ANN trained with SUB2 exhibited a slightly lower correlation coefficient ($R \simeq 0.66$) but smaller error (RMSE $\simeq$ 9 cm) when tested on SUB1, while the other ANN shown higher

correlation (R ≃ 0.74) but also higher error (RMSE ≃ 11.5 cm) with some saturation for highest SD values that were not properly represented in the training. This analysis confirmed that, if the training is representative enough of the snowpack properties, the ANN can be successfully applied to other datasets (in our case to another period of the same winter season).

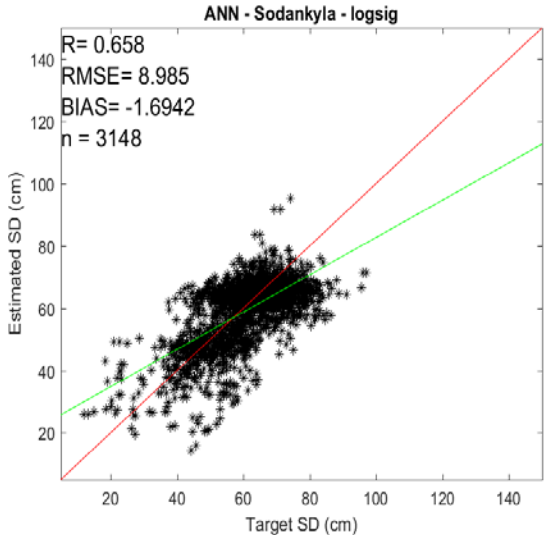

a)

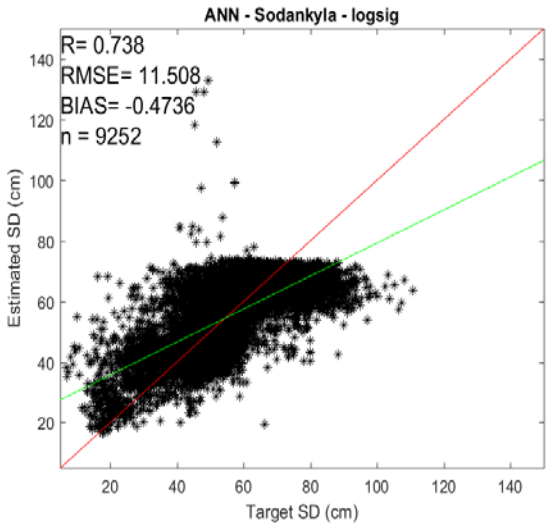

b)

Fig. 9. a) validation on mission 1-5 of the ANN trained with missions 6-10, b) validation on mission 6-10 of the ANN trained with missions 1-5.

4) Algorithm robustness over space: Canada test case

The algorithm robustness was also verified over space by applying the ANN trained with the Finland dataset to the Canada dataset. The obtained results (R= 0.65 – RMSE≃12 cm) confirmed the feasibility of the proposed approach, provided again that the training was sufficiently representative of the entire set of observed snowpack conditions.

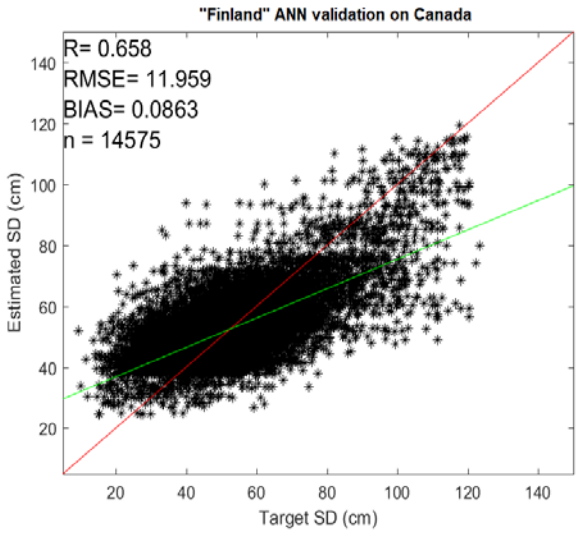

Fig. 10. Validation of the "Finland" ANN on the Canada dataset.

5) Single channel algorithm

The feasibility of retrieving SD by only using the Ku band channel was also evaluated. For this scope, another ANN has been implemented and trained according to the strategy described in section IV.A, but considering only the Ku band data at both polarizations. The validation result is shown in FIG. 11.

As expected, the decrease in accuracy is evident, especially in terms of correlation (R≃0.73), while the RMSE of about 14 cm is not far from the result of the general algorithm shown in Fig. 6. This analysis confirms the contribution of X band in improving the retrieval, thus suggesting the effectiveness of the approach proposed for the CoReH2O mission.

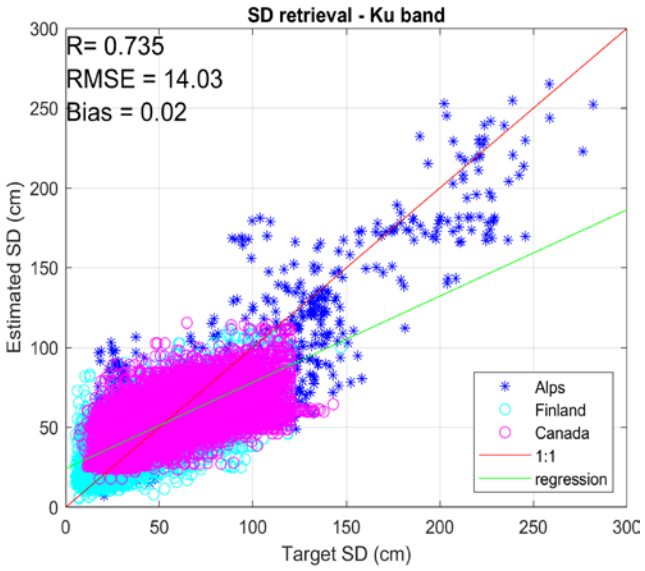

Fig. 11. Validation of the "single frequency" ANN using Ku band data only.

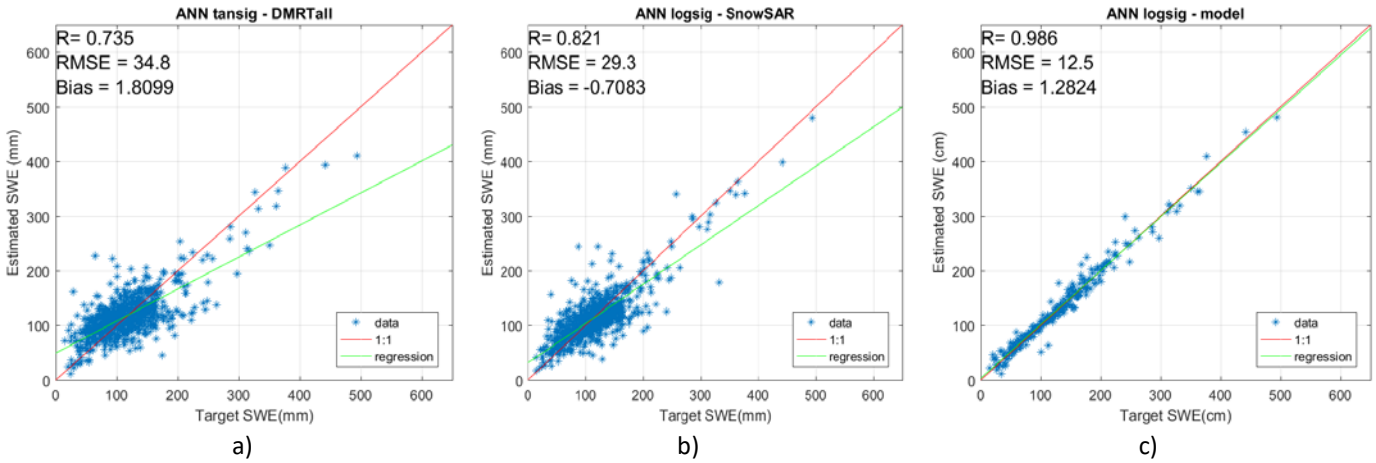

Fig. 12. Validation of the "model driven" approach: a) SWE estimated by the ANN trained with DMRT-QMS plotted as a function of the target values from in-situ, b) result of the ANN trained and tested with experimental data, c) result of the ANN trained and tested with simulated data.

B. Model driven approach: ANN trained with DMRT-QMS

The validation of ANN trained with DMRT-QMS (ANN_{DMRT}) is shown in Fig. 12 a), where the SWE estimated by the ANN is represented as a function of the SWE from in-situ. As a term of comparison, the result obtained by training the ANN with the same subset of SnowSAR measurements corresponding to the DMRT-QMS simulations ($ANN_{SnowSAR}$) is shown in Fig. 12 b): the main statistics are R ≃ 0.74, RMSE ≃ 35 mm and bias ≃ 2 mm for ANN_{DMRT} and R ≃ 0.82, RMSE ≃ 29 mm and bias < -0.7 mm for $ANN_{SnowSAR}$. Finally, Fig. 12 c) shows the result when ANN is trained and tested with DMRT-QMS simulated data. Fig. 12 demonstrates that the accuracy of the model driven implementation in estimating SWE is not far from the one of experimental driven implementation, especially in terms of RMSE. The lower correlation can be attributed to the light disagreement between SnowSAR data and DMRT-QMS simulations at Ku band (Fig. 4), since Fig. 12 c) demonstrates that the ANN is able to invert DMRT-QMS almost exactly.

The obtained results suggest the effectiveness of the "model driven" training. Improvements in the input parametrization of DMRT-QMS and, especially, a better characterization of the soil surface contribution to the total backscatter, can further improve the retrieval accuracy. Concerning the Alpine datasets, although some studies pointed out a successful capability of DMRT-QMS in simulating data collected on Alps [8], other authors [48] reported model inaccuracies that could represent an issue to address in some specific cases.

VI. DISCUSSION

This study had the twofold purpose of analysing the SnowSAR dataset as a whole and to provide a methodology for SWE/SD retrieval based on X + Ku SAR acquisitions, along with proofs of its effectiveness. In this respect, two retrieval approaches, data driven and model driven have been proposed. The validation of data driven approach was conducted on a relevant part of the dataset (50%) not involved in the training and demonstrated the capability of the ANN algorithms to retrieve SD from the SnowSAR acquisitions, with R ≃ 0.77. The correlation analysis pointed out that training and validation datasets were almost independent (R<0.3), thus ensuring the representativeness of the validation results.

The robustness of the algorithm was also evaluated over time and over space considering some subsets of the entire dataset: the results confirmed the effectiveness of the data driven approach.

The model driven retrieval based on DMRT-QMS obtained similar accuracies (R≃0.74). This method had the double advantage of reducing the amount of experimental data required for training the algorithm and of filling in the gaps of experimental datasets. The model simulations allowed obtaining a training set representative of a variety of observed conditions that the SnowSAR data cannot reproduce, although collected in extremely different environmental conditions.

The results shown in section V.B suggest that by improving the DMRT-QMS input parametrization and especially by better accounting for the soil background contribution, the model driven approach can provide even more accurate retrievals. Further investigations should therefore focus on improving the DMRT-QMS input parametrization and modeling of soil background. Such improvement could be not always straightforward, especially for specific cases as the high Alpine terrain and glacier test sites of AlpSAR. Moreover, opportunities to perform multi-year ANN tests should be investigated, to verify the applicability of training data from preceding years for retrievals in consecutive seasons and, in conclusion, to further assess the reliability of this method for implementing an unsupervised inversion algorithm aimed at estimating SD and SWE from multifrequency SAR acquisitions. In this respect, it should be mentioned that updating the training with new data is quite straightforward, as it does not imply any change of the algorithm structure, so that the proposed approach can be updated for extending the ANN applicability to new datasets, hopefully collected by future satellite sensors.

VII. Conclusions

The analysis of the SnowSAR backscattering ($\sigma°$) sensitivity to SD, carried out on the entire dataset in dry snow conditions, pointed out some increase of the measured $\sigma°$ when SD increases at both frequencies and polarizations. However, the spatial and temporal variations of microstructure and density of snow, and soil characteristics, may have a dominant effect on such sensitivity.

The way that each soil and snow parameter affected the measured σ^0 changes depended on frequency and polarization: therefore, the retrieval problem was addressed by exploiting the synergy of available polarizations and frequencies.

In this respect, the potential of machine learning applications and in particular of Artificial Neural Networks (ANN) was evaluated: ANN have been selected among other retrieval techniques because they can combine easily input data from different sources, thus being particularly suitable for combining the two frequencies and two polarizations of SnowSAR in the same retrieval algorithm.

This study focused on SD retrieval because the amount of SWE data available from the in-situ measurements was not sufficient for completing successfully the ANN training and testing operations, while a large number of SD samples were available from manual measurements. It is well known indeed that ANN need of large training sets for obtaining reliable retrievals. In this case, the algorithm was trained on 50% of the entire dataset (i.e. over the three tests site) of SnowSAR acquisitions and corresponding in situ SD measurements, while the remaining 50% of data was used for validating the trained ANN, by predicting SD from SnowSAR acquisitions not involved in the training.

The results obtained with this approach, with a correlation coefficient $R \simeq 0.77$ between estimated and target SD, a root-mean-square error (RMSE) $\simeq$ 13 cm, and a bias negligible, suggested that ANN are an effective instrument for addressing the retrieval. The investigated possibility of training the algorithm with data simulated by the Dense Medium Radiative Transfer (DMRT), also resulted in comparable accuracies ($R \simeq 0.74$ and RMSE $\simeq$35 mm of SWE) with the twofold advantage of reducing the amount of in-situ data needed for the training, and extending the algorithm exportability to other test sites.

VIII. References

[1] WMO - Global Telecommunication System webpage http://www.wmo.int/pages/prog/www/TEM/GTS/index_en.html. (2017)

[2] Hall, D. K., G. A. Riggs, and V. V. Salomonson. 2006. MODIS/Terra Snow Cover 5-Min L2 Swath 500m. Version 5. Boulder, Colorado USA: NASA National Snow and Ice Data Center Distributed Active Archive Center. http://dx.doi.org/10.5067/ACYTYZB9BEOS.

[3] Kelly R. E., A. T. Chang, Leung Tsang and J. L. Foster, "A prototype AMSR-E global snow area and snow depth algorithm," in IEEE Transactions on Geoscience and Remote Sensing, vol. 41, no. 2, pp. 230-242, Feb. 2003. doi: 10.1109/TGRS.2003.809118.

[4] Takala M, K. Luojus, J. Pulliainen, C. Derksen, J. Lemmetyinen, J-P. Kärnä, J. Koskinen, and B. Bojkov (2011). Estimating northern hemisphere snow water equivalent for climate research through assimilation of space-borne radiometer data and ground-based measurements. Remote Sens. Environ., 115(12), 3517-3529.

[5] Tedesco, M., and J. Jeyaratnam, 2016: A new operational snow retrieval algorithm applied to historical AMSR-E brightness temperatures. Remote Sens., 8, no. 12, 1037, doi:10.3390/rs8121037.

[6] Tedesco, M., J. Jeyaratnam and R. Kelly. 2019. NRT AMSR2 Unified L3 Global Daily 25 km EASE-Grid Snow Water Equivalent. Dataset available online from the NASA Global Hydrology Resource Center DAAC, Huntsville, Alabama, U.S.A. DOI: http://dx.doi.org/10.5067/AMSRU/AU_DySno_NRT_R01

[7] Guneriussen, T., K. A. Hogda, H. Johnson, and I. Lauknes (2001). InSAR for estimating changes in snow water equivalent of dry snow. IEEE Trans. Geosci. Rem. Sens., 39(10), 2101-2108.

[8] Pettinato S., E. Santi, M. Brogioni, S. Paloscia, E. Palchetti, and Chuan Xiong, 2013, The Potential of COSMO-SkyMed SAR Images in Monitoring Snow Cover Characteristics, IEEE Geoscience and Remote Sensing Letters, 10, 1, pp.9-13.

[9] Leinss, S., A. Wiesmann, J., Lemmetyinen, and I. Hajnsek (2015). Snow water equivalent of dry snow measured by differential interferometry. IEEE J. Sel. Top. Appl. Earth Observ. Remote Sens., 8(8), 3773–3790, http://dx.doi.org/10.1109/JSTARS.2015.2432031.

[10] Leinss, S., G. Parrella, and I. Hajnsek (2014). Snow height determination by polarimetric phase differences in X-band SAR data. IEEE J. Sel. Topics Appl. Earth Observ. Remote Sens., 7, 3794-3810.

[11] Lievens, Hans, Matthias Demuzere, Hans-Peter Marshall, Rolf H. Reichle, Ludovic Brucker, Isis Brangers, Patricia de Rosnay et al. "Snow depth variability in the Northern Hemisphere mountains observed from space." Nature communications 10, no. 1 (2019): 1-12.

[12] Rott, H., S. Yueh, D. Cline, C. Duguay, R. Essery, C. Haas, F. Hélière, M. Kern, G. Macelloni, E. Malnes, T. Nagler, J. Pulliainen, H. Rebhan, and A. Thompson, 2010. Cold Regions Hydrology High-Resolution Observatory for Snow and Cold Land Processes, Proc. IEEE, 98(5), 752-765.

[13] Coccia A., C. Trampuz, E. Imbembo and A. Meta, “First Results of SnowSAR, the new X-and Ku-Band Polarimetric Airborne SAR Sensor supporting the CoReH2O Mission”, Workshop on Advanced RF Sensors and Remote Sensing Instruments, ESA/ESTEC, Noordwijk, NL, 13-15 Sept. 2011.

[14] Di Leo D, Coccia A, Meta A (2015) Technical Assistance for the Development and Deployment of an

X-and Ku-band MiniSAR Airborne System (SnowSAR). ESTEC No. 4000106761-CCN1.

[15] King, J., C. Derksen, P. Toose, A. Langlois, C. Larsen J. Lemmetyinen, P. Marsh, B. Montpetit, A. Roy, N. Rutter, and M. Sturm, 2018. The influence of snow microstructure on dual-frequency radar measurements in a tundra environment. Remote Sens. Environ., 215, 242-254, ISSN 0034-4257

[16] Hannula H., J. Lemmetyinen, A: Kontu, C. Derksen, and J. Pulliainen, 2016. Spatial and temporal variation of bulk snow properties in northern boreal and tundra environments based on extensive field measurements, Geosci. Instrum. Method. Data Syst., 5, 347-363, doi:10.5194/gi-5-347-2016.

[17] Rott H., T. Nagler, R. Prinz, K. Voglmeier, R. Fromm et al.: AlpSAR 2012-13, a field experiment on snow observations and parameter retrievals with Ku- and X-band radar. Proc. of ESA Living Planet Symposium, ESA SP-722, 8pp., 2013.

[18] Lemmetyinen, J., J. Pulliainen, A. Kontu, A. Wiesmann, C. Mätzler, H. Rott, K. Voglmeier, T. Nagler, A. Meta, A. Coccia, M. Schneebeli, M. Proksch, M. Davidson, D. Schüttemeyer, Chung-Chi Lin, and M. Kern, 2014. Observations of seasonal snow cover at X- and Ku bands during the NoSREx campaign. Proc. EUSAR 2014, 3-5 June 2014, Berlin.

[19] Lemmetyinen, J., J. Pulliainen, A. Kontu, A. Wiesmann, C. Mätzler, H. Rott, K. Voglmeier, T. Nagler, A. Meta, A. Coccia, M. Schneebeli, M. Proksch, M. Davidson, D. Schüttemeyer, Chung-Chi Lin, and M. Kern, 2014. Observations of seasonal snow cover at X- and Ku bands during the NoSREx campaign. Proc. EUSAR 2014, 3-5 June 2014, Berlin.

[20] Zhu, J. S. Tan, J. King, C. Derksen, J. Lemmetyinen, and L. Tsang, 2018. Forward and Inverse Radar Modeling of Terrestrial Snow Using SnowSAR Data. IEEE Trans. Geosci. Remote Sens., 56, 12, 7122-7132. DOI: 10.1109/TGRS.2018.2848.

[21] Xu X., L. Tsang, S. Yueh, "Electromagnetic Models of Co/Cross-polarization of Bicontinuous/DMRT in Radar Remote Sensing of Terrestrial Snow at X- and Ku-band for CoReH2O and SCLP Applications," Selected Topics in Applied Earth Observations and Remote Sensing, IEEE Journal of, vol. 5, no. 3, pp. 1024-1032, June 2012.

[22] Ding K. H., X. Xu, and L. Tsang, "Electromagnetic scattering by bicontinuous random microstructures with discrete permittivities," IEEE Trans. Geosci. Remote Sensing, vol. 48, no. 8, pp. 3139–3151, 2010.

[23] Rott H., D. W. Cline, C. Duguay, R. Essery, P. Etchevers, I. Hajnsek, M. Kern, G. Macelloni, E Malnes, J. Pulliainen, S.H. Yueh., "CoReH2O, a dual frequency radar mission for snow and ice observations," 2012 IEEE International Geoscience and Remote Sensing Symposium, Munich, 2012, pp. 5550-5553, doi: 10.1109/IGARSS.2012.6352348.

[24] Ma L., Y. Liu, X. Zhang, Y. Ye, G. Yin, B. A. Johnson, Deep learning in remote sensing applications: A meta-analysis and review, ISPRS Journal of Photogrammetry and Remote Sensing, Volume 152, 2019, Pages 166-177, ISSN 0924-2716, https://doi.org/10.1016/j.isprsjprs.2019.04.015.

[25] Hornik K., M. Stinchcombe and H. White, "Multilayer feedforward network are universal approximators," Neural Networks, vol. 2, no. 5, pp. 359–366, 1989.

[26] Linden A.and J. Kinderman, "Inversion of multi-layer nets," in Proc. Int. Joint Conf. Neural Networks, vol. 2, pp. 425–430.

[27] Baghdadi N., S. Gaultier & C. King (2002) Retrieving surface roughness and soil moisture from synthetic aperture radar (SAR) data using neural networks, Canadian Journal of Remote Sensing, 28:5, 701-711, DOI: 10.5589/m02-066.

[28] Del Frate F., P. Ferrazzoli and G. Schiavon, "Retrieving soil moisture and agricultural variables by microwave radiometry using neural networks," Remote Sens. Environ., vol. 84, no. 2, pp. 174–183, Feb. 2003.

[29] Elshorbagy A. and K. Parasuraman, On the relevance of using artificial neural networks for estimating soil moisture content,Journal of Hydrology, Volume 362, Issues 1, 2008, Pages 1-18, ISSN 0022-1694, https://doi.org/10.1016/j.jhydrol.2008.08.012.

[30] Paloscia S., P. Pampaloni, S. Pettinato and E. Santi, "A comparison of algorithms for retrieving soil moisture from ENVISAT/ASAR images," IEEE Tran. Geosci. Remote Sens., vol. 46, no. 10, pp. 3274-3284, Oct. 2008.

[31] Dai X., Z. Huo, H. Wang, Simulation for response of crop yield to soil moisture and salinity with artificial neural network, Field Crops Research, Volume 121, Issue 3, 2011, Pages 441-449, ISSN 0378-4290, https://doi.org/10.1016/j.fcr.2011.01.016.

[32] Santi E. 2016. Neural Networks applications for the retrieval of hydrological parameters from microwave satellite sensors. Artificial Neural Networks - Models and Applications book, InTechOpen, ISBN 978-953-51-2705-5.

[33] Tsang L., J. Pan, D. Liang, Z. X. Li, D. Cline, and Y. H. Tan, 2007. Modeling active microwave remote sensing of snow using dense media radiative transfer (DMRT) theory with multiple scattering effects, IEEE Trans. Geosci. Remote Sens., 45, no. 4, pp. 990–1004.

[34] Liang D., Xiaolan Xu, L. Tsang, K.M. Andreadis, E.G. Josberger, "The Effects of Layers in Dry Snow on Its Passive Microwave Emissions Using Dense Media Radiative Transfer Theory Based on the Quasicrystalline Approximation (QCA/DMRT)", IEEE Trans. Geosci. Remote Sensing, vol. 46, pp. 3663–3671, 2008.

[35] Cohen J., J. Lemmetyinen, J. Pulliainen, K. Heinilä, F. Montomoli, J. Seppänen, and M. T. Hallikainen, "The effect of boreal forest canopy in satellite snow mapping - A multisensor analysis," IEEE Trans. Geosci. Remote Sens., vol. 53, no. 12, pp. 6593–6607, Dec. 2015

[36] Rott, H., T. Nagler, E. Ripper, K. Voglmeier, R. Prinz, R. Fromm, A. Coccia, A., A. Meta, D. Di Leo and D.

Schüttemeyer, 2014. Ku- and X-band backscatter analysis and SWE retrieval for Alpine snow. Proc. of 2014 IEEE Int. Geoscience & Remote Sensing Symp., ISBN 978-1-4799-5775-0, pp. 2407-2410.

[37] Paloscia S., S. Pettinato, E. Santi, C. Notarnicola, L. Pasolli, A. Reppucci, 2013, “Soil moisture mapping using Sentinel-1 images: Algorithm and preliminary validation”, Remote Sensing of Environment, 134, pp. 234-248, doi.org/10.1016/j.rse.2013.02.027.

[38] Santi E., S. Paloscia, S. Pettinato and G. Fontanelli. “Application of artificial neural networks for the soil moisture retrieval from active and passive microwave spaceborne sensors,” Int. J. Appl. Earth Observ. Geoinf., vol 48, pp. 61–73, Jun. 2016.

[39] Tarpanelli, A., Santi, E., Tourian, M.J., Filippucci, P., Amarnath, G., Brocca, L.; Daily River Discharge Estimates by Merging Satellite Optical Sensors and Radar Altimetry Through Artificial Neural Network. (2019) IEEE Transactions on Geoscience and Remote Sensing, 57 (1), art. no. 8424052, pp. 329-341. DOI: 10.1109/TGRS.2018.2854625

[40] Research Resources webpage, university of Michigan, 2015. http://web.eecs.umich.edu/~leutsang/Available Resources.html.

[41] Löwe H. and G. Picard. 2015: Microwave scattering coefficient of snow in MEMLS and DMRT-ML revisited: the relevance of sticky hard spheres and tomography-based estimates of stickiness. The Cryosphere, 9, pp. 2101.

[42] Oh, Y., Sarabandi, K., Ulaby, F. T. 1992. An empirical model and an inversion technique for radar scattering from bare surfaces, IEEE Transactions on Geoscience and Remote Sensing, 30, 370-381.

[43] Lemmetyinen, J., Kontu, A., Pulliainen, J., Vehviläinen, J., Rautiainen, K., Wiesmann, A., Mätzler, C., Werner, C., Rott, H., Nagler, T., Schneebeli, M., Proksch, M., Schüttemeyer, D., Kern, M., and Davidson, M. W. J.: Nordic Snow Radar Experiment, Geosci. Instrum. Method. Data Syst., 5, 403-415, https://doi.org/10.5194/gi-5-403-2016, 2016.

[44] Fierz, C., Armstrong, R. L., Durand, Y., Etchevers, P., Greene, E., McClung, D. M., Nishimura, K., Satyawali, P. K., and Sokratov, S. A.: The International Classification for Seasonal Snow on the Ground. IHP-VII Technical Documents in Hydrology no. 83, IACS contribution no. 1, UNESCO-IHP, Paris, 2009.

[45] Chang W., S. Tan, J. Lemmetyinen, L. Tsang, X. Xu and S. H. Yueh, "Dense Media Radiative Transfer Applied to SnowScat and SnowSAR," in IEEE Journal of Selected Topics in Applied Earth Observations and Remote Sensing, vol. 7, no. 9, pp. 3811-3825, Sept. 2014. doi: 10.1109/JSTARS.2014.2343519

[46] Mironov V. L., R. D. De Roo, I. V. Savin, "Temperature-dependable microwave dielectric model for an arctic soil", IEEE Trans. Geosci. Remote Sens., vol. 48, no. 6, pp. 2544-2556, Jun. 2010.

[47] Montomoli F., G. Macelloni, M. Brogioni, J. Lemmetyinen, J. Cohen and H. Rott, "Observations and Simulation of Multifrequency SAR Data Over a Snow-Covered Boreal Forest," in IEEE Journal of Selected Topics in Applied Earth Observations and Remote Sensing, vol. 9, no. 3, pp. 1216-1228, March 2016. doi: 10.1109/JSTARS.2015.2417999.

[48] Nagler, T., H. Rott, M. Heidinger, J. Pulliainen, G. Macelloni, F. Montomoli, and D. Flach, 2012. CoReH2O Algorithm Theoretical Basis Document (ATBD), Deliv. 7, V1.9, ESA ESTEC Contract No. 22830/09/NL/JC, 31 Oct. 2012.